A new interpretation of sea-surface slope probability density functions

William J. Plant

Applied Physics Laboratory, University of Washington, Seattle, Washington, USA

Received 25 March 2003; revised 4 June 2003; accepted 19 June 2003; published 13 September 2003.

[1] Sea-surface slope probability density functions, which are usually fitted to a Gram-Charlier series, can be fit equally well by a bound wave/free wave model in which the distributions of bound and free waves are Gaussian. Bound waves are generated by longer waves on the surface and travel at nearly the phase speed of the long wave while free waves are generated directly by the wind and travel at their intrinsic phase speed. These two types of short surface waves can usually be separated in measurements that yield their velocities. The integrals over the two distributions yield the probabilities of finding bound or free waves on the surface. We show that the probability of finding bound waves on the ocean is comparable to that in a wind-wave tank and much larger than the probability of whitecapping. The mean slopes of the two distributions yield the mean tilts of bound or free waves. We show that the mean tilt of the bound waves is similar to that in a wind-wave tank and close to that necessary to explain Doppler shifts in microwave backscatter from the sea surface at high incidence angles. Finally, the widths of the two distributions yield the variance of sea-surface slopes at the locations of bound and free waves. We show that these are larger at sea than in a wind-wave tank, which explains why bound waves at sea have not been recognized previously in sea-surface slope probability distributions. *INDEX TERMS:* 4560 Oceanography: Physical: Surface waves and tides (1255); 4504 Oceanography: Physical: Air/sea interactions (0312); 4506 Oceanography: Physical: Capillary waves; *KEYWORDS:* bound waves, sea-surface slopes, probability density functions

Citation: Plant, W. J., A new interpretation of sea-surface slope probability density functions, *J. Geophys. Res.*, *108*(C9), 3295, doi:10.1029/2003JC001870, 2003.

1. Measurements and Previous Interpretations

[2] The classic measurements of sea-surface slopes by *Cox and Munk* [1954] using sun glitter patterns determined the basic characteristics of these slopes. Many other measurements have confirmed and extended the results of Cox and Munk [*Hughes et al.*, 1977; *Tang and Shemdin*, 1983; *Haimbach and Wu*, 1985; *Hwang and Schemdin*, 1988; *Wu*, 1991; *Shaw and Churnside*, 1997]. These measurements indicate that when wind and waves are aligned, the cross wind probability density function (PDF) is nearly Gaussian while the upwind/downwind PDF differs significantly from Gaussian. The latter PDF shows a shift of the peak of the spectrum toward downwind slopes, an increase in the tail of the distribution in the upwind direction, and an increase in peak height relative to a Gaussian PDF with the same variance. Figure 1 illustrates this behavior with a fit to one of the PDFs measured by Cox and Munk at a wind speed of 10.2 m/s. Note that we have changed the sign of the slope compared to Cox and Munk since this became common practice in later papers by other authors. It is essential to be clear on the definition of "upwind" and "downwind" slopes in interpreting these measured PDFs. "Downwind" (here, positive) means that the sea surface height increases in the wind direction, that is, the vector normal to the surface is tilted in the upwind direction.

[3] The traditional method of interpreting upwind/downwind slope PDFs has been to fit them to a Gram-Charlier series, which can be derived by assuming that surface waves are weakly nonlinear [*Longuet-Higgins*, 1963a]. *Cox and Munk* [1954, 1956] gave this series as a function of upwind/downwind and cross wind slope. Integrating their expression over the cross wind slope yields

$$P(s) = G(s)[1 + (c_3/6)H_3 + (c_4/24)H_4], \tag{1}$$

where s is the upwind/downwind slope, and $G(s)$ is a Gaussian distribution,

$$G(s) = \frac{1}{\sigma\sqrt{2\pi}} \exp\left(\eta^2/2\right), \tag{2}$$

where σ is the RMS upwind/downwind slope and

$$\eta = \frac{s - \langle s \rangle}{\sigma}, \tag{3}$$

where $\langle s \rangle$ is the mean slope. For the sea surface as a whole, this is taken to be zero. H_n is the nth Hermite polynomial,

0148-0227/03/2003JC001870$09.00

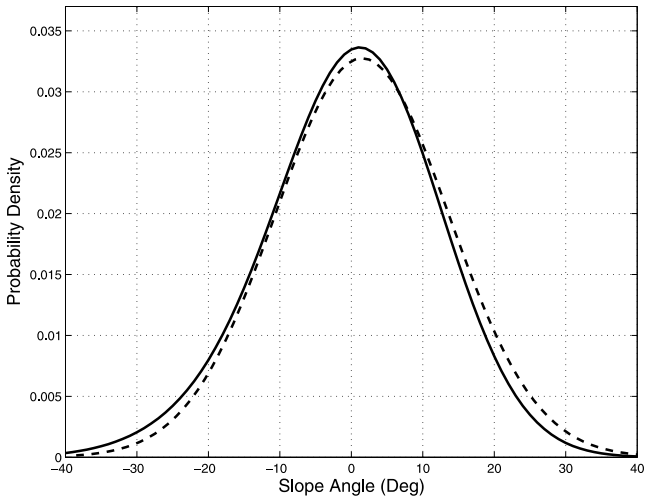

Figure 1. Comparison of an upwind/downwind sea-surface slope PDF fit by *Cox and Munk* [1954] to their optical data (solid curve) with a Gaussian PDF having the same variance (dashed curve). Downwind slopes are positive. The wind speed at 12.5 m height was 10.2 m/s.

the first five of which are given in Table 1. The coefficients c_n of this series are calculated from the difference in the moments of $P(s)$ and $G(s)$,

$$c_n = \frac{1}{\sigma^n} \int s^n [P(s) - G(s)] ds. \tag{4}$$

[4] Fitting the PDF to this form, of course, gives no physical insight into the causes of its shape beyond the fact that nonlinearities must exist. *Longuet-Higgins* [1982] attempted to give such insight by considering three possible effects: small, nonlinear distortions of individual waves, viscous damping of free waves, and the modulation of ripples. He found that only the modulation of ripples by longer waves could yield skewnesses, c_3, of the correct magnitude and sign. His interpretation of the mathematics yielding this result was that the modulation of the ripples by the long waves caused an increase in ripple amplitude on the forward (leeward) face of the long wave. The slope of the long waves then shifted these increased ripple slopes toward the upwind direction, thus increasing the tail of the distribution in this direction. Since the tails of the distribution predominantly affect the skewness, this gave the correct sign.

[5] We propose here a different interpretation of the sea-surface slope PDF. As in Longuet-Higgins' interpretation, the shape of the PDF is again determined by the characteristics of the ripples. We propose, however, that it is not primarily the modulation of ripples by longer waves that skews the PDF but the generation of ripples by longer waves.

2. Interpretation Using Bound and Free Waves

[6] A model of the sea surface involving wind waves and bound, tilted waves has proven to be very successful in explaining microwave backscatter from wind-roughened water surfaces [*Plant*, 1997; *Plant et al.*, 1999a, 1999b]. In addition to long waves, this model postulates ripples that cover the whole sea surface but are generated in two different ways: directly by the wind, or by longer wind waves. The former ripples propagate at their intrinsic phase speed, that predicted by linear wave theory augmented slightly by wind drift and nonlinear effects; we call these free waves. The other type of ripple is generated by longer waves on the surface and travels at, or near, the phase speed of these longer waves; we call these bound waves. The two types of ripples are generally easily separated by a measurement capable of determining their speed, such as high speed optical measurements or the scattering of coherent microwave or acoustic radiation [*Plant*, 1997; *Hara et al.*, 1997; *Plant et al.*, 1999a; *Rozenberg et al.*, 1999]. Exceptions to this statement are parasitic capillary waves, which we consider to be a subset of bound waves because they travel at the phase speed of their parent waves. However, the condition for generation of a parasitic capillary wave is that this speed also be its intrinsic phase speed [*Longuet-Higgins*, 1963b; *Fedorov and Melville*, 1998]. Therefore they travel at the same speed as free waves. However, they are preferentially located on the tilted, forward face of their parent wave so their effect on the local incidence angle of microwave scattering above the surface and on acoustic scattering below the surface may be different and allows their identification [*Plant et al.*, 1999b]. Other types of small-scale surface roughness that we would classify as bound waves are nonlinear distortions of longer waves and turbulent regions due to breaking or crumpling waves [*Longuet-Higgins*, 1992; *Duncan et al.*, 1994, 1999].

[7] In order to derive sea-surface slope PDFs from this model, we assume that free and bound waves may be considered independently. This seems a reasonable assumption since the turbulence in front of the crest of gravity waves probably accounts for most bound waves and cannot be related to the random wind wave field in general. If the bound waves are parasitic or due to breaking or crumpling, we assume that they damp free waves at that location to the point of insignificance. Thus their mean slope can be very different from the free waves. In fact, if bound wave slopes are skewed in one direction, then free wave slopes must be skewed in the other in order that the mean slope of the sea surface be zero. Smaller nonlinear distortions of longer waves, of course, exist at the same place on the surface as the wind waves and so must have the same mean slope. Such small distortions are important only at low wind speeds where their effect is not overshadowed by parasitic, breaking, or crumpling waves.

[8] The overall sea-surface slope PDF, P_{fb}, given by this model is obtained using Bayes theorem,

$$P_{fb}(s) = P_f P(s|f) + P_b P(s|b), \tag{5}$$

where P_f is the probability of finding a free wave at a particular location on the sea surface, P_b is the probability of

Table 1. Hermite Polynomials

n	$H_n(\eta)$
0	1
1	η
2	$\eta^2 - 1$
3	$\eta^3 - 3\eta$
4	$\eta^4 - 6\eta^2 + 3$

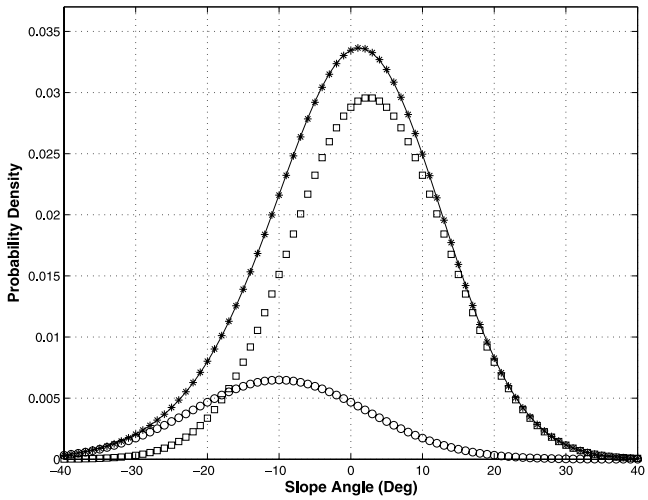

Figure 2. Comparison of sea-surface slope PDF fits with a Gram-Charlier series and with a free/bound wave model. The solid curve is the Gram-Charlier fit, the squares are P_f times the free-wave PDF, the circles are P_b times the bound-wave PDF, and the asterisks are the sum of the circles and squares. The wind speed at 12.5 m height was 13.5 m/s for this PDF.

finding a bound wave, and $P(s|f)$ and $P(s|b)$ are the conditional probabilities of slopes where free and bound waves exist, respectively. Here and later, subscripts f and b refer to free and bound waves. This equation immediately yields

$$1 = P_f + P_b. \tag{6}$$

Furthermore, all moments of the distribution, and therefore c_3 and c_4 can be calculated from equations (4) and (5), with $P(s)$ replaced by $P_{fb}(s)$, by assuming that the conditional probabilities $P(s|f)$ and $P(s|b)$ are Gaussian.

$$0 = P_f\langle s_f\rangle + P_b\langle s_b\rangle, \tag{7}$$

$$\sigma^2 = P_f\left(\sigma_f^2 + \langle s_f\rangle^2\right) + P_b\left(\sigma_b^2 + \langle s_b\rangle^2\right), \tag{8}$$

Table 2. Parameters of Gram-Charlier Series That Fit Measured Sea-Surface Slopes PDFs as Given by *Cox and Munk* [1956][a]

U(12.5), m/s	σ (CM)	c_3 (CM)	c_4 (CM)	c_3	c_4
13.3	0.0484	−0.463	0.215	−0.370	0.219
13.8	0.0452	−0.220	0.177	−0.220	0.177
13.7	0.0404	−0.345	0.177	−0.276	0.028
0.72	0.0005	0.101	0.127	0.091	0.117
8.58	0.0230	−0.165	0.027	−0.132	0.028
3.93	0.0098	0.003	0.129	0.024	0.048
8.00	0.0191	−0.156	0.173	−0.156	0.173
6.30	0.0170	−0.143	0.101	−0.143	0.102
6.44	0.0186	−0.148	0.129	−0.148	0.130
4.92	0.0174	−0.080	−0.019	−0.064	−0.019
10.2	0.0357	−0.283	0.128	−0.255	0.129
11.7	0.0374	−0.105	0.172	−0.116	0.172
9.79	0.0264	−0.180	0.084	−0.162	0.085
9.74	0.0322	−0.407	0.128	−0.326	0.134
10.5	0.0365	−0.600	0.196	−0.420	0.197

[a]Values of skewness, c_3, and kurtosis, c_4 may be compared with those from this study, which are given in the last two columns.

$$c_3 = \left[P_f\left(3\langle s_f\rangle\sigma_f^2 + \langle s_f\rangle^3\right) + P_b\left(3\langle s_b\rangle\sigma_b^2 + \langle s_b\rangle^3\right)\right]/\sigma^3, \tag{9}$$

$$c_4 = \left[P_f\left(3\sigma_f^4 + 6\sigma_f^2\langle s_f\rangle^2 + \langle s_f\rangle^4\right) + P_b\left(3\sigma_b^4 + 6\sigma_b^2\langle s_b\rangle^2 + \langle s_b\rangle^4\right)\right]/\sigma^4 - 3. \tag{10}$$

The assumption that the conditional probabilities are Gaussian is weakest for the bound waves since these are, by definition, finite amplitude effects of free waves and could themselves exhibit finite amplitude properties. For lack of definite knowledge of these properties, however, we will maintain the Gaussian assumption.

[9] The latter five equations contain six parameters relating to free and bound waves: P_f, P_b, $\langle s_f\rangle$, $\langle s_b\rangle$, σ_f, and σ_b. We have fit this model to Cox and Munk's PDFs by using the first four of these equations to eliminate all parameters but P_b and $\langle s_b\rangle$ from the expression for P_{fb}. We then varied the value of c_3 and found its value and the values of P_b and $\langle s_b\rangle$ that minimized a cost function given by

$$C = 100\left(P - P_{fb}\right)^2 + \left(c_4 - c_{4cm}\right)^2, \tag{11}$$

where c_4 comes from equation (10) and c_{4cm} is *Cox and Munk*'s [1956] value of c_4. The first term requires that the best-fit PDF P_{fb} match P while the second term requires that the fourth moments of the PDFs also match. The factor of 100 is necessary to give nearly equal weight to the two terms in C. We tried using C without the second term but found that a wide range of P_b and $\langle s_b\rangle$ existed over which the cost function had nearly the same value. Adding the second term reduced this range so that a clear minimum is obtained. To determine P, the Gram-Charlier fit to the data,

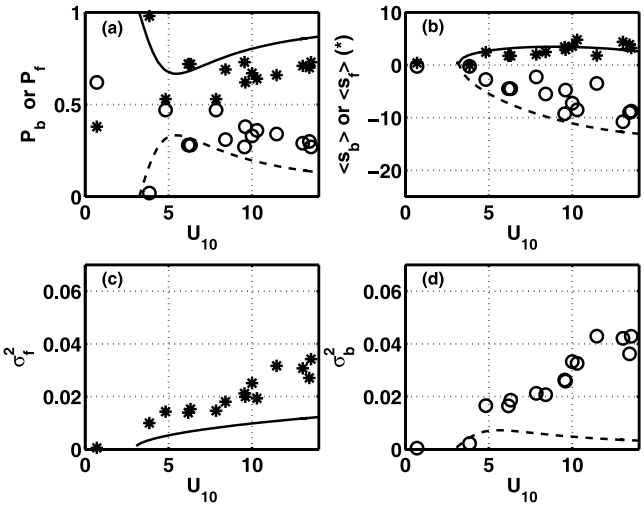

Figure 3. Bound and free wave parameters versus wind speed at 10 m height. Symbols were deduced from fits to the *Cox and Munk* [1954, 1956] data and therefore represent ocean data. In Figures 3a and 3b, asterisks correspond to free waves and open circles are bound wave values. Curves show best fits to results obtained in a wind-wave tank [*Plant et al.*, 1999a].

we used the data of *Cox and Munk* [1956] that corresponded to wind and waves aligned to within 20°. We found that minimizing C always produced excellent fits to P. A representative example is shown in Figure 2. Table 2 gives Cox and Munk's parameters determined from their data along with the values we determined here for c_3 and c_4. Both c_3 and c_4 are very close to those of Cox and Munk.

3. Properties of Bound and Free Waves

[10] The six parameters determined by this fitting procedure have very definite physical meanings. They yield the probabilities of finding the different types of ripples, their mean slopes, and the variances of these slopes. We examined the behavior of these properties of bound and free waves as a function of wind speed and compared them with those determined in a wind-wave tank by *Plant et al.* [1999a]. The results are shown in Figure 3. Here U_{10} was determined for the tank measurements by dividing measured friction velocities by $\sqrt{0.00115}$ and for Cox and Munk's measurements by dividing their wind speeds at 12.5 m by 1.02. Clearly, the probability of finding bound waves on the ocean is comparable to that in the wind-wave tank. This probability is much larger than that of whitecapping, indicating that many bound waves are microbreakers that do not entrain air [*Monahan*, 1971]. The mean slopes of free and bound waves are also very similar in the tank and on the ocean. *Plant et al.* [1999a] showed that the mean slopes of the bound waves and their spectral densities determined from optical measurements were just slightly smaller in magnitude than those necessary to explain microwave backscatter observations in the wind-wave tank. Similarly, the magnitudes of the mean slopes of the bound waves at sea that have been determined here are somewhat less than the 20° tilts necessary to explain Doppler shifts in microwave backscatter from the ocean at high incidence angles [*Plant*, 1997]. Interestingly, the variances of the free waves determined in this 1997 study do not differ markedly from those found here but the bound wave variances do. Figures 3c and 3d show that both of these variances are higher at sea than in the wavetank, presumably due to the presence of much longer waves on the ocean. These large variances relative to the mean slopes make signatures of bound waves at sea more difficult to recognize than they are in a wind-wave tank.

[11] **Acknowledgments.** This work was supported by the Space and Remote Sensing program of the Office of Naval Research under grants N00014-00-1-0075 and N00014-01-1-0153.

References

Cox, C., and W. Munk, Statistics of the sea surface derived from sun glitter, *J. Mar. Res.*, *13*(2), 199–227, 1954.

Cox, C., and W. Munk, Slopes of the sea surface deduced from photographs of sun glitter, *Bull. Scripps Inst. Oceanogr.*, *6*, 401–488, 1956.

Duncan, J. H., V. Philomin, M. Behres, and J. Kimmel, The formation of spilling breaking water waves, *Phys. Fluids*, *6*, 2558–2560, 1994.

Duncan, J. H., H. Qiao, V. Philomin, and A. Wenz, Gentle spilling breakers: Crest profile evolution, *J. Fluid Mech.*, *379*, 191–222, 1999.

Fedorov, A. W., and W. K. Melville, Nonlinear gravity-capillary waves with forcing and dissipation, *J. Fluid Mech.*, *354*, 1–42, 1998.

Haimbach, S. P., and J. Wu, Field trials of an optical scanner for studying sea-surface fine structures, *IEEE J. Ocean. Eng.*, *OE-10*(4), 451–453, 1985.

Hara, T., E. J. Bock, and M. Donelan, Frequency-wavenumber spectrum of wind-generated gravity-capillary waves, *J. Geophys. Res.*, *102*(C1), 1061–1072, 1997.

Hughes, B. A., H. L. Grant, and R. W. Chappell, A fast response surface-wave slope meter and measured wind-wave moments, *Deep Sea Res.*, *24*, 1211–1223, 1977.

Hwang, P. A., and O. H. Shemdin, The dependence of sea surface slope on atmospheric stability and swell conditions, *J. Geophys. Res.*, *93*(C11), 13,903–13,912, 1988.

Longuet-Higgins, M. S., The effect of non-linearities on statistical distributions in the theory of sea waves, *J. Fluid Mech.*, *17*, 459–480, 1963a.

Longuet-Higgins, M. S., The generation of capillary waves by steep gravity waves, *J. Fluid Mech.*, *16*, 138–159, 1963b.

Longuet-Higgins, M. S., On the skewness of sea-surface slopes, *J. Phys. Oceanogr.*, *12*, 1283–1291, 1982.

Longuet-Higgins, M. S., Capillary rollers and bores, *J. Fluid Mech.*, *240*, 659–679, 1992.

Monahan, E. C., Oceanic whitecaps, *J. Phys. Oceanogr.*, *1*, 139–144, 1971.

Plant, W. J., A model for microwave Doppler sea return at high incidence angles: Bragg scattering from bound, tilted waves, *J. Geophys. Res.*, *102*(C9), 21,131–21,146, 1997.

Plant, W. J., W. C. Keller, V. Hesany, T. Hara, E. Bock, and M. Donelan, Bound waves and Bragg scattering in a wind wavetank, *J. Geophys. Res.*, *104*(C2), 3243–3263, 1999a.

Plant, W. J., P. H. Dahl, and W. C. Keller, Microwave and acoustic scattering from parasitic capillary waves, *J. Geophys. Res.*, *104*(C11), 25,853–25,866, 1999b.

Rozenberg, A. D., M. J. Ritter, and W. K. Melville, Free and bound capillary waves as microwave scatterers: Laboratory studies, *IEEE Trans. Geosci. Remote Sens.*, *37*(2), 1052–1065, 1999.

Shaw, J. A., and J. H. Churnside, Scanning-laser glint measurements of sea-surface slope statistics, *Appl. Opt.*, *36*(18), 4202–4213, 1997.

Tang, S., and O. H. Shemdin, Measurement of high frequency waves using a wave follower, *J. Geophys. Res.*, *88*(C14), 9832–9840, 1983.

Wu, J., Effects of atmospheric stability on ocean rippler: A comparison between optical and microwave measurements, *J. Geophys. Res.*, *96*(C4), 7265–7269, 1991.

W. J. Plant, Applied Physics Laboratory, University of Washington, 1013 Northeast 40th Street, Seattle, WA 98105-6698, USA. (plant@apl.washington.edu)